

Magnetocrystalline anisotropy of FePt: a detailed view

Saleem Ayaz Khan,¹ Peter Blaha,² Hubert Ebert,³ Jan Minár,^{1,3} and Ondřej Šipr^{1,4}

¹*New Technologies Research Centre, University of West Bohemia,
Univerzitní 2732, 306 14 Pilsen, Czech Republic*

²*Institute of Materials Chemistry, TU Vienna, Getreidemarkt 9, A-1060 Vienna, Austria*

³*Universität München, Department Chemie, Butenandtstr. 5-13, D-81377 München, Germany*

⁴*Institute of Physics ASCR v. v. i., Cukrovarnická 10, CZ-162 53 Prague, Czech Republic*

(Dated: July 17, 2022)

To get a reliable accurate value for the magneto-crystalline anisotropy (MCA) energy of FePt within the local density approximation (LDA) to the density functional theory, we employ the full-potential linearized augmented plane wave (FLAPW) method as implemented in the WIEN2k code and the full-potential Korringa-Kohn-Rostoker (KKR) Green function method as implemented in the SPRKKR code. If both calculations are properly converged, the same MCA energy is obtained — even though the codes use different approaches to deal with the spin-orbit coupling (SOC). As the calculated MCA energy (3.4 meV) significantly differs from experiment (1.3 meV), it is clear that many-body effects beyond the LDA are important. By analyzing the dependence of the MCA energy on the magnetization angle and on the SOC we show that the main mechanism of MCA in FePt can be described within the framework of second order perturbation theory. However, a significant contribution not accountable for by second order perturbation theory is present as well.

Keywords: magnetism; anisotropy; relativity

I. INTRODUCTION

The various ab-initio electronic structure codes use different approaches to solve the Schrödinger equation for a solid. Usually different codes and/or methods yield results that are similar but show sometimes important differences in the details. These details start to matter if one aims at high-precision calculations with predictive power. Therefore an effort has lately intensified to standardize ab-initio calculations and to find the conditions that have to be met so that reliable “true” quantitative values are obtained. So far the attention has been paid mostly to total energies, equilibrium lattice parameters and bulk moduli.^{1–4} We want to extend this effort to another numerically sensitive area, namely, to the magneto-crystalline anisotropy (MCA). The MCA is manifested by the fact that the energy of a magnetically ordered material depends on the direction of the magnetization

\mathbf{M} with respect to the crystal lattice. It is an interesting phenomenon both for fundamental and technological reasons, as the MCA is important among others for the design of magnetic recording media.^{5,6}

Getting an accurate value of the MCA energy E_{MCA} is quite difficult as one has to, at least in principle, subtract two very large numbers (total energies for two orientations of magnetization) to get a very small number, namely, E_{MCA} . Several conditions for getting accurate well-converged results were explored in the past. In particular, the importance of a sufficiently dense mesh in the Brillouin zone (BZ) for the \mathbf{k} -space integration was recognized.^{7–9} When dealing with supported systems such as adatoms or monolayers, the semi-infinite substrate has to be properly accounted for.^{10,11} Despite all the efforts, getting accurate and reliable theoretical predictions of the MCA energy is still a problem.

In this work we focus on MCA of bulk FePt. This com-

pound has the largest MCA energy of all bulk materials formed by transition metals and its crystal structure is quite simple, so it is a good candidate for a reliable calculation. At the same time, the presence of Pt — a heavy element — suggests that relativistic effects should be significant, offering thus an interesting possibility to check how different methods of dealing with relativistic effects, in particular with the spin-orbit coupling, influence the results.

Previous theoretical studies on FePt based on the local density approximation (LDA) give a large spread of the results — from 1.8 meV to 4.3 meV.^{8,12–19} If one restricts to full potential methods only, one still gets a relatively large difference between various studies: E_{MCA} of FePt was determined as 2.7 meV by FP-LMTO calculation of Ravindran *et al.*⁸ and FLAPW calculation of Shick and Mryasov,¹⁷ 3.1 meV by plane-waves calculation of Kosugi *et al.*²⁰ and 3.9 meV by FP-LMTO calculation of Galanakis *et al.*¹⁶ The differences between various LDA calculations are comparable to the differences between LDA results and the experimental value of 1.3 meV.²¹ Even though part of the spread of the LDA results can be attributed to the use of different LDA exchange-correlation functionals, the differences are still too large to be acceptable. Besides, they occur also for studies which use the same exchange-correlation functional (e.g., both Ravindran *et al.*⁸ and Galanakis *et al.*¹⁶ use von Barth and Hedin functional).²² This suggests that the accuracy of ab-initio MCA energy calculations may not be sufficient to answer a simple question such as whether the LDA itself is able to reproduce the experimental MCA energy of FePt or not.

Deciding which method gives better MCA results than the other is quite difficult, among others because different computational approaches used by different codes are intertwined with different ways of implementing relativistic effects. Recall that as the MCA is intimately related to the spin orbit coupling (SOC), which is a relativistic effect, the way the relativity is included can be an impor-

tant factor. Reckoning all of this, reliable MCA energy can only be obtained if one uses two different methods and each of them yields the same value after being properly converged. Then one can be sure that the MCA energy thus obtained is indeed “method independent” and represents the correct quantum-mechanical result.

The aim of our work is to perform a robust and accurate LDA calculation of the MCA energy of FePt to get a definite answer to the question whether the MCA of FePt can be described within the LDA scheme or not and to establish a benchmark against which other LDA calculations could be checked. The first computational method we employ is the well-established and recognized full potential linearized augmented plane wave (FLAPW) method as implemented in the WIEN2k code.²³ This method was used as a reference in the recent study of the accuracy of total energies and related quantities.^{1–3} As the second method we opted for a fully relativistic multiple scattering KKR (Korringa-Kohn-Rostoker) Green function formalism as implemented in the SPRKKR code.^{24,25} We will show in the following that if both methods are properly converged, they yield same values for the MCA energy (3.4 meV). This is significantly larger than the experimental value (1.3 meV), implying conclusively that the LDA cannot properly describe the MCA of FePt.

Many aspects of the MCA of FePt were theoretically investigated in the past already. Daalderop *et al.*¹² and Ravindran *et al.*⁸ studied the influence of the band-filling on E_{MCA} of FePt. Many groups studied the influence of the temperature on the MCA of FePt.^{26,27} The dependence of the Curie temperature on the FePt grain size was investigated via model Hamiltonian calculations.²⁸ Burkert *et al.*,¹⁹ Lukashev *et al.*²⁹ and Kosugi *et al.*²⁰ studied how E_{MCA} depends on the strain (i.e., the c/a ratio). Cuadrado *et al.*³⁰ gradually substituted the Fe atom by Cr, Mn, Co, Ni, or Cu to find that the MCA energy of $\text{Fe}_{1-y}\text{X}_y\text{Pt}$ alloys can be tuned by adjusting the content of the substituting element.

To facilitate the understanding of the MCA of FePt

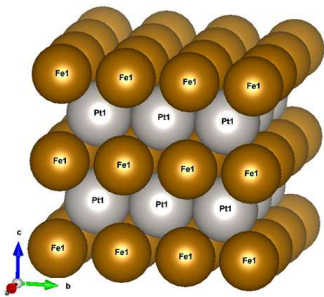


FIG. 1. Crystal structure of bulk $L1_0$ FePt

further, we focus on some aspects that have not been paid attention so far. In particular, we assess how different ways of dealing with relativistic effects influence magnetic moments and densities of states. We also analyze how the total energy varies with the magnetization angle and how MCA energy scales with spin-orbit coupling. Based on this we assess to what degree the mechanism leading to the MCA in FePt can be described within second order perturbation theory.

II. COMPUTATIONAL DETAILS

We studied bulk FePt with the $L1_0$ layered structure. The lattice parameters of a $tP2$ unit cell are $a=2.722$ Å and $c=3.714$ Å. Fe atoms and Pt atoms are at the $(0.0,0.0,0.0)$ and $(0.5,0.5,0.5)$ crystallographic positions, respectively, resulting in a compound with alternating Fe and Pt atomic layers stacked along the c axis (see Fig. 1).

We used two different computational methods, namely, the FLAPW method as implemented in the WIEN2k code²³ and the multiple scattering KKR Green function method as implemented in the SPRKKR code.^{24,25} Our calculations are based on the LDA. The values presented in the section Results (Sec. III) were obtained using the Vosko, Wilk and Nusair (VWN) exchange-correlation functional.³¹ Use of different LDA functionals leads to small but identifiable changes in E_{MCA} , as explored in Sec. III E.

The KKR Green function calculations were done mostly in the full-potential (FP) mode; sometimes

the atomic spheres approximation (ASA) was employed (Sec. III D). The energy integrals were evaluated by contour integration on a semicircular path within the complex energy plane, using a Gaussian mesh of 40 points. An important convergence parameter is the maximum angular momentum $\ell_{\max}^{(KKR)}$ used for the multipole expansion of the Green function (see Appendix 1). To get accurate results, we mostly use $\ell_{\max}^{(KKR)}=5$. However, if a lot of calculations with different settings has to be done (Secs. III C and III D) we use $\ell_{\max}^{(KKR)}=3$, which is sufficient if the focus is on how E_{MCA} varies with the magnetization angle or with the SOC strength and not on particular values.

The convergence of FLAPW calculations is determined by the size of the basis. We treated Fe $3p$, $3d$, $4s$ and Pt $5p$, $5d$, $6s$ states as valence states and Fe $1s$, $2s$, $2p$, $3s$ and Pt $1s$, $2s$, $2p$, $3s$, $3p$, $3d$, $4s$, $4p$, $4d$, $4f$, $5s$ states as core states. The expansion of the wave functions into plane waves is controlled by the plane wave cutoff in the interstitial region. This cutoff is specified via the product $R_{MT}K_{\max}$, where R_{MT} is the smallest muffin-tin (“atomic”) sphere radius and K_{\max} is the magnitude of the largest wave vector. We use $R_{MT}K_{\max}=8$ in this study. The convergence of E_{MCA} with $R_{MT}K_{\max}$ is investigated in Appendix 2. The expansion of the wave functions into atomic-like functions inside the spheres is controlled by the angular-momentum cutoff $\ell_{\max}^{(APW)}$. We use $\ell_{\max}^{(APW)}=10$ throughout this paper. Note that the cutoff’s $\ell_{\max}^{(APW)}$ and $\ell_{\max}^{(KKR)}$ have different roles in FLAPW and KKR-Green function methods, so their values cannot be directly compared.

As concerns the muffin-tin radii in WIEN2k calculations, the atomic spheres are chosen so that they are smaller than the touching spheres for the MCA energy calculations ($R_{MT}^{(Fe)}=2.2$ a.u., $R_{MT}^{(Pt)}=2.3$ a.u., $R_{MT}^{(touch)}=2.527$ a.u.) because in this way the basis avoids the linearization error. On the other hand, for analyzing site-related magnetic moments we use touching muffin-tin spheres because in this way we minimize the moments

associated to the interstitial region. In this way we are in a better position to compare the WIEN2k results with the SPRKKR data, where the site-related magnetic moments are determined as moments within Voronoi polyhedra. The stability of E_{MCA} with respect to R_{MT} 's variation is demonstrated in Appendix 3.

Once the Green function components or the wave functions have been determined, the charge density is obtained via the \mathbf{k} -space integration over the BZ. The integration mesh is another important convergence parameter, common to both methods. All results presented in this study were obtained using 100000 \mathbf{k} -points in the full BZ. The convergence of E_{MCA} with respect to the number of \mathbf{k} -points is explored in Appendix 4.

A. Treatment of relativistic effects

The SPRKKR code works fully relativistically, it solves a four-component Dirac equation by default. SOC is therefore implicitly fully included for all states. Nevertheless, the bare effect of the SOC can be investigated via SPRKKR if one employs an approximate two-component scheme³² where the SOC-related term is identified by relying on a set of approximate radial Dirac equations. This scheme was used recently to investigate how the MCA energy of adatoms and monolayers on noble metals varies if SOC is selectively switched on only at some sites.¹¹ We employed it here for the same purpose.

As concerns the WIEN2k code, SOC is included differently for core and valence electrons. The core electrons are treated fully relativistically by solving the atomic-like Dirac equation. For the valence electrons the SOC is included in atomic spheres via an approximative scheme that introduces an additional term

$$H_{SOC} = \xi(\mathbf{r}) \mathbf{L} \cdot \mathbf{S} \quad (1)$$

to the spin-polarized Schrödinger-like scalar relativistic equation. Technically, the influence of the term (1) is included by starting with a scalar-relativistic FLAPW cal-

culcation without SOC. The eigenfunctions thus obtained are then used as a basis in which another diagonalization is done and this time also the SOC term Eq. (1) is taken into account. This procedure is often called second variational step.³³ Usually this second variational step is applied only to a subset of FLAPW eigenstates to gain a substantial speed-up. This subset is defined so that it includes all scalar-relativistic eigenstates up to energy E_{max} above the Fermi level. The E_{max} parameter thus plays an analogous role as $R_{MT}K_{max}$. Moreover, relativistic local orbitals ($p_{1/2}$ wavefunctions) were added to the basis.³⁴ To achieve the highest accuracy, we set E_{max} as large as needed to include all FLAPW eigenfunctions in the second step (this can be achieved by setting E_{max} of 100 Ry or higher). More details can be found in Appendix 5. As concerns the interstitial region, valence electrons are treated in a non-relativistic way. In the rest of this paper “fully relativistic calculation” implies use of the Dirac equation for SPRKKR and Schrödinger equation plus separate SOC term (1) in the Hamiltonian for WIEN2k.

The SPRKKR and WIEN2k codes allow for non-relativistic and scalar-relativistic calculations as well. In the first case, both valence and core electrons are treated non-relativistically. In the second case, the valence electrons are treated using the scalar-relativistic approach while for the core electrons atomistic Dirac equation is solved (this applies to both codes).

B. Scaling of the spin-orbit coupling

For a deeper understanding we want to investigate how E_{MCA} depends on the SOC. More specifically, we are interested in how E_{MCA} varies if the SOC strength is varied at the Fe and Pt sites separately, i.e., we assume that the Hamiltonian Eq. (1) can be symbolically rewritten as

$$H_{SOC} = \sum_i \lambda^{(i)} \xi^{(i)}(\mathbf{r}) \mathbf{L}^{(i)} \cdot \mathbf{S}^{(i)} \quad , \quad (2)$$

TABLE I. Spin magnetic moments (in μ_B) related either to a FePt unit cell or just to the Fe site, for different ways of including the relativistic effects.

	SPRKKR		WIEN2k	
	$\mu_{\text{spin}}^{(\text{cell})}$	$\mu_{\text{spin}}^{(\text{Fe})}$	$\mu_{\text{spin}}^{(\text{cell})}$	$\mu_{\text{spin}}^{(\text{Fe})}$
non relativistic	3.18	2.87	3.15	2.86
scalar relativistic	3.23	2.88	3.21	2.87
fully relativistic	3.19	2.85	3.17	2.84

TABLE II. Orbital magnetic moments (in μ_B) related to the Fe and Pt atoms in FePt for magnetization either parallel to the z axis ($\mu_{\text{orb}}^{(M\parallel z)}$) or perpendicular to the z axis ($\mu_{\text{orb}}^{(M\parallel x)}$).

	Fe		Pt	
	SPRKKR	WIEN2k	SPRKKR	WIEN2k
$\mu_{\text{orb}}^{(M\parallel z)}$	0.064	0.065	0.043	0.042
$\mu_{\text{orb}}^{(M\parallel x)}$	0.062	0.062	0.060	0.054

where $\lambda^{(i)}$ is the scaling factor for site i . Such calculations were done via the SPRKKR code, using the approximate scheme³² mentioned in the beginning of Sec II A.

III. RESULTS

A. Magnetic moments

The presence of Pt in FePt suggests that the way relativistic effects are treated could be important. To investigate this, we calculated magnetic moments in FePt using a non-relativistic Schrödinger equation, using a scalar-relativistic approach, and using a relativistic scheme. Spin magnetic moments related either to the unit cell or only to the Fe site are shown in Tab. I. We can see that relativity has only a marginal effect on the spin magnetic moments in FePt. Orbital magnetic moments are more interesting in this respect — they would be zero in the absence of SOC. Our results in Table II give the orbital magnetic moment at the Fe and Pt sites for two orientations of the magnetization.

One can see that both codes lead to very similar values

for μ_{spin} and μ_{orb} . In particular, the anisotropy of μ_{orb} at Fe and at Pt sites is nearly the same. Small differences between the codes in the local magnetic moments may be due to the fact that they are defined in different regions: Wigner-Seitz cells (or more precisely Voronoi polyhedra) in SPRKKR and touching muffin-tin spheres in WIEN2k. The difference would be larger if we used “standard” setting of muffin-tin radii in WIEN2k ($R_{\text{MT}}^{(\text{Fe})}=2.2$ a.u. and $R_{\text{MT}}^{(\text{Pt})}=2.3$ a.u. instead of $R_{\text{MT}}^{(\text{Fe})}=R_{\text{MT}}^{(\text{Pt})}=2.527$ a.u.): in that case, the local spin moments obtained via WIEN2k would be smaller by about 3 % and orbital moments by about 10 %.

B. Magneto-crystalline anisotropy energy

Calculating the MCA energy by subtracting total energies for two orientations of the magnetization is very sensitive and challenging, because the total energies and the MCA energy differ by about eight or nine orders of magnitude. We paid a lot of attention to the issues of convergence to get accurate numbers. The details can be found in the appendix. Here we only mention two technical parameters which have to be given special attention. For full-potential SPRKKR calculations it is the cutoff for multipole expansion of the Green function $\ell_{\text{max}}^{(\text{KKR})}$ (we used $\ell_{\text{max}}^{(\text{KKR})}=5$). For WIEN2k calculations it is E_{max} which controls how many scalar-relativistic eigen-states are considered when SOC is included (we used $E_{\text{max}}=100$ Ry meaning that all eigen-states were included). The MCA energy obtained by subtracting the total energies,

$$E_{\text{MCA}} \equiv E^{(M\parallel x)} - E^{(M\parallel z)} \quad , \quad (3)$$

is shown in the first line of Tab. III. Values obtained via SPRKKR and WIEN2k show good agreement. This, together with the careful convergence analysis we performed, allows us to state with confidence that the magnetic easy axis of FePt is out-of-plane and the MCA energy is close to 3.4 meV within the LDA framework (for the VWN exchange-correlation functional).

TABLE III. MCA energy E_{\max} of FePt (in meV) calculated by three different approaches.

	SPRKKR	WIEN2k
subtracting total energies	3.40	3.39
magnetic force theorem	3.42	2.97
Bruno formula	-2.64	-2.09

Obtaining the MCA energy by subtracting the total energies is computationally very costly. The need for self-consistent calculations for two magnetization directions can be avoided if one relies on the magnetic force theorem. In this approach the MCA energy is calculated using a frozen spin-dependent potential.³⁵ The MCA energy is then obtained either by subtracting the band-energies or by evaluating the torque at magnetization tilt angle of 45° (Refs. 36–38). As the magnetic force theorem is frequently employed, we applied it here as well. The results are shown in the second line of Tab. III. We can see that the magnetic force theorem yields practically identical values as if total energies are subtracted for the SPRKKR code while there are small but significant deviations for the WIEN2k code. It is not clear what is the reason for this — let us just note that we used identical technical parameters for both WIEN2k calculations.

For the sake of completeness we checked also the Bruno formula,³⁹

$$E_{\text{MCA}} = \sum_i \frac{\xi^{(i)}}{4} \left(\mu_{\text{orb}}^{(i, \mathbf{M} \parallel z)} - \mu_{\text{orb}}^{(i, \mathbf{M} \parallel x)} \right), \quad (4)$$

which links the MCA energy to the anisotropy of orbital magnetic moments of constituting atoms labeled by i (cf. analogous equation in Ravindran *et al.*)⁸ The Bruno formula³⁹ (as well as the slightly more sophisticated van der Laan formula)⁴⁰ can be derived from second order perturbation theory if some additional assumptions are made: Bruno formula assumes that the minority-spin band is fully occupied and both formulas assume that spin-flip processes can be neglected. It is often employed in the context of x-ray magnetic circular dichroism ex-

periments that give access to the anisotropy of orbital magnetic moment via the so-called sum rules. We evaluated it here using SOC parameters $\xi^{(\text{Fe})}=65$ meV and $\xi^{(\text{Pt})}=712$ meV. These values were obtained from ab-initio calculations for FePt relying on the method described by Davenport *et al.*,⁴¹ as implemented in the SPRKKR code. Practically the same values are obtained also for Fe and Pt elemental crystals.

The results for the Bruno formula are presented in the third line of Tab. III. The sign of E_{MCA} evaluated from Eq. (4) is wrong, indicating that the Bruno formula does not provide a suitable framework for studying the MCA of FePt. Technically, the reversal of the sign of E_{MCA} obtained via Eq. (4) is due to μ_{orb} at Pt (see Tab. II): we have $\mu_{\text{orb}}^{(\mathbf{M} \parallel z)} > \mu_{\text{orb}}^{(\mathbf{M} \parallel x)}$ at the Fe site and $\mu_{\text{orb}}^{(\mathbf{M} \parallel x)} > \mu_{\text{orb}}^{(\mathbf{M} \parallel z)}$ at the Pt site. As $\xi^{(\text{Pt})}$ is much larger than $\xi^{(\text{Fe})}$, the Pt-related term dominates in Eq. (4).

The failure of the Bruno formula does not automatically imply that second order perturbation theory cannot be used for describing the MCA of FePt. It may be that the additional assumptions employed in the derivation of Eq. (4) are not fulfilled. Two more indicative tests whether second order perturbation theory provides a good framework for understanding the MCA of FePt are presented below.

C. Dependence of the total energy on the orientation of the magnetization axis

Accurate calculations can provide information on the full functional dependence of the total energy on the angle θ between the magnetization direction and the z axis. For tetragonal systems the first two terms in the directional cosines expansion of the total energy are

$$E(\theta) - E_0 = K_1 \sin^2 \theta + K_2 \sin^4 \theta \quad . \quad (5)$$

Here we omit the azimuthal dependence, keeping $\phi=0^\circ$. If the influence of SOC is included via the explicit term Eq. (1), then application of second order perturbation

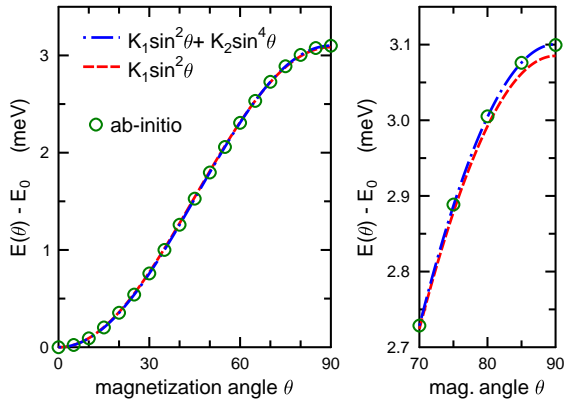


FIG. 2. Dependence of the total energy on the magnetization angle θ (circles) and its fit either as $K_1 \sin^2 \theta$ (dashed line) or as $K_1 \sin^2 \theta + K_2 \sin^4 \theta$ (dash-dotted line). An overall view is in the left panel, a detailed view on the region close to $\theta=90^\circ$ is in the right panel.

theory leads to a purely uniaxial dependence of the total energy on the angle θ , meaning that only the first term survives in Eq. (5).^{39,42} Inspecting the full $E(\theta)$ dependence as obtained via fully-relativistic ab-initio calculations thus provides the possibility to estimate to what degree a treatment of MCA based on second order perturbation theory is adequate: large K_2 coefficient implies large deviations from second order perturbation theory.

We performed a series of calculations for different magnetization tilt angle θ using the SPRKKR code in the full-potential mode. The MCA energy was evaluated as a difference of total energies. The results are shown via circles in Fig. 2. Because we wanted to have a fine θ -mesh, we had to perform a lot of calculations; therefore, we used $\ell_{\max}^{(\text{KKR})}=3$ in this section. The numerical value for $\theta=90^\circ$ thus differs a bit from Tab. III, where the $\ell_{\max}^{(\text{KKR})}=5$ cutoff was used.

The ab-initio data were fitted via Eq. (5). If only the $K_1 \sin^2 \theta$ term is employed (taking $K_2=0$), we obtain $K_1=3.085$ meV. If both terms in Eq. (5) are employed, we obtain $K_1=3.008$ meV and $K_2=0.092$ meV. Even though both fits look nearly the same in the over-

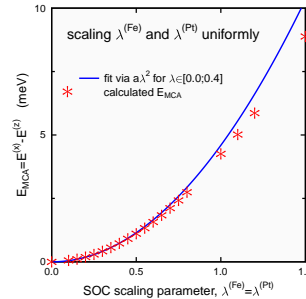


FIG. 3. Dependence of E_{MCA} on the SOC scaling factor λ .

all view, a detailed analysis shows that the fit with both terms is significantly better (cf. the right panel in Fig. 2). Using even higher order terms in the fit did not lead to a significant improvement. We conclude, therefore, that the MCA of FePt is almost purely axial, with a small identifiable higher-order contribution.

D. Dependence of the MCA energy on spin orbit coupling

If the magnetocrystalline anisotropy is described within second order perturbation theory, it scales with the square of the SOC-scaling parameter λ , $E_{\text{MCA}} \sim \lambda^2$ (Refs. 39, 40, and 42). Inspecting the $E_{\text{MCA}}(\lambda)$ dependence thus provides another criterion to what degree second order perturbation theory is sufficient to describe magnetocrystalline anisotropy of FePt. We calculated E_{MCA} using the scheme described in Sec. II B for a uniform SOC scaling, i.e., for $\lambda^{(\text{Fe})} = \lambda^{(\text{Pt})} = \lambda$ [cf. Eq. (2)] while varying λ from 0 to 1.5 to cover the non-relativistic as well as the relativistic regime: if λ is zero, there is no spin orbit coupling, if λ is 1, we recover the standard relativistic case. Evaluation of E_{MCA} was done by subtracting total energies. To reduce the computer requirements, we performed all the calculations presented in this section with $\ell_{\max}^{(\text{KKR})}=3$ in the ASA mode; this enables us to use a fine λ mesh so that the curve fitting is reliable. The results are shown by points in Fig. 3. Employment of the ASA leads to less accurate results than

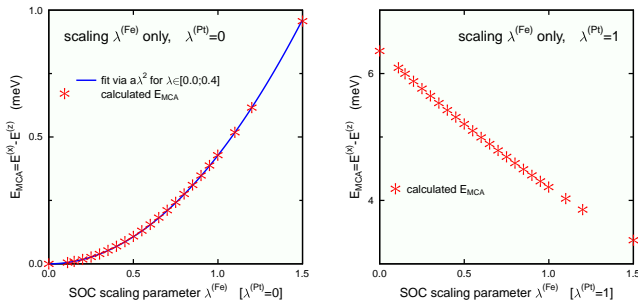


FIG. 4. Dependence of E_{MCA} on the SOC scaling factor at the Fe sites $\lambda^{(Fe)}$.

for FP calculations (E_{MCA} obtained within the ASA is by 1.1 eV larger than E_{MCA} obtained for full potential). However, this does not affect our conclusions concerning the scaling of E_{MCA} with strength of the SOC.

As concerns the fitting of the $E_{MCA}(\lambda)$ dependence, we want to employ it for verifying the prediction of the perturbation theory. Perturbation theory should work well for small values of the parameter λ while it can be less appropriate for large values of λ . So the fit to the

$$E_{MCA}(\lambda) = a\lambda^2 \quad (6)$$

function is performed in such a way that the a coefficient is sought only for λ in the range between zero and 0.4 (the upper value was arbitrarily chosen just for convenience). One can see from Fig. 3 that while the fit describes the ab-initio data very well within the $\lambda \in [0; 0.4]$ range, there are small but clear deviations for larger λ . This suggests that while second order perturbation theory accounts for the dominant mechanism of magnetocrystalline anisotropy of FePt, some effects beyond it are also significant.

To learn more, we explore the effect of scaling the SOC at the Fe and Pt sites separately. When varying $\lambda^{(Fe)}$ or $\lambda^{(Pt)}$ we further distinguish two cases — either the SOC at the remaining species is totally suppressed ($\lambda = 0$) or it is kept at its “normal” value ($\lambda = 1$). Results for scaling SOC at the Fe sites are shown in Fig. 4, results for scaling SOC at the Pt sites are shown in Fig. 5. Fits to the quadratic dependence of E_{MCA} on $\lambda^{(Fe)}$ or on $\lambda^{(Pt)}$

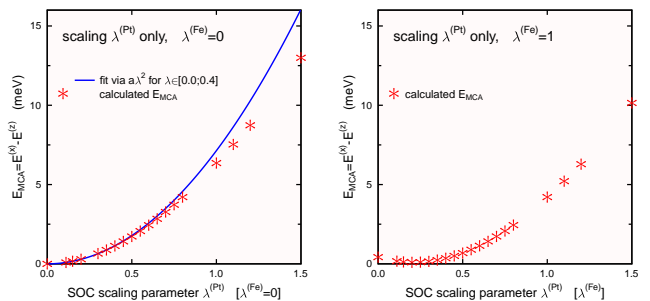


FIG. 5. Dependence of E_{MCA} on the SOC scaling factor at the Pt sites $\lambda^{(Pt)}$.

were done only in case that SOC at the other site is suppressed. Namely, only then we get zero E_{MCA} for $\lambda^{(i)}=0$ and fitting $E_{MCA}(\lambda^{(i)})$ with Eq. (6) thus makes sense. Similarly as in the case of the uniform scaling, the fits were attempted for $\lambda^{(i)}$ in the $[0; 0.4]$ interval.

Concerning the case when SOC is varied at the Fe sites, one can see that if $\lambda^{(Pt)}=0$, the dependence of E_{MCA} on $\lambda^{(Fe)}$ is perfectly accounted for by second order perturbation theory: the quadratic fit describes the $E_{MCA}(\lambda^{(Fe)})$ dependence very well also outside the $[0; 0.4]$ interval in which the a coefficient was sought (left graph in Fig. 4). This suggests that it must be the strong SOC at Pt sites which makes the $E_{MCA}(\lambda)$ curve in Fig. 3 to deviate from a perfect parabola. Indeed, if SOC at Pt sites is switched on (right graph in Fig. 4), a quite unexpected *decline* of E_{MCA} with increasing $\lambda^{(Fe)}$ is observed.

Let us turn now to the case of varying $\lambda^{(Pt)}$. If there is no SOC at the Fe sites, the $E_{MCA}(\lambda^{(Pt)})$ dependence is described by the fitted parabola only for low values of $\lambda^{(Pt)}$ (left graph in Fig. 5). If $\lambda^{(Pt)}$ increases beyond the fitting interval of $[0; 0.4]$, deviations of ab-initio data points from the fit by Eq. (6) are similar as for uniform SOC fit presented in Fig. 3. So it follows from our analysis that the effect of SOC at the Fe sites can be accounted for by second order perturbation theory while the effect of SOC at the Pt sites goes beyond it.

TABLE IV. The MCA energy of FePt (in meV) calculated by means of the magnetic force theorem for different exchange and correlation functionals.

	SPRKKR	WIEN 2k
Vosko and Wilk and Nusair ³¹	3.42	2.97
Perdew and Wang ⁴³	-	2.90
von Barth and Hedin ²²	3.57	3.13
Moruzzi, Janak and Williams ⁴⁴	3.38	-

E. Dependence of the MCA energy on the LDA exchange-correlation functional

Usually the calculated properties of solids do not crucially depend on which form of the LDA exchange-correlation functional is used. However, as the MCA energy is a very sensitive quantity, it is useful to investigate how the E_{MCA} varies if different LDA exchange-correlation functionals are used. Apart from the VWN exchange-correlation functional used throughout this work we include in this comparison the Perdew and Wang exchange-correlation functional⁴³ (the default for WIEN2k) and functionals suggested by von Barth and Hedin²² and by Moruzzi, Janak and Williams.⁴⁴

We evaluated E_{MCA} by means of the magnetic force theorem for this test. The results are summarized in Tab. IV. One can see that different LDA functionals lead to MCA energies that differ from each other by 0.1–0.2 meV.

F. Relativistic effects in the density of states

Fig. 6 shows how relativity affects the density of states (DOS) resolved in angular momentum components respective to Fe and Pt sites. The data presented here were obtained using the SPRKKR code (in the FP mode); data obtained using the WIEN2k code look practically the same. Generally, there is a significant change in the DOS when going from non-relativistic to scalar-relativistic case and only a minor change when going

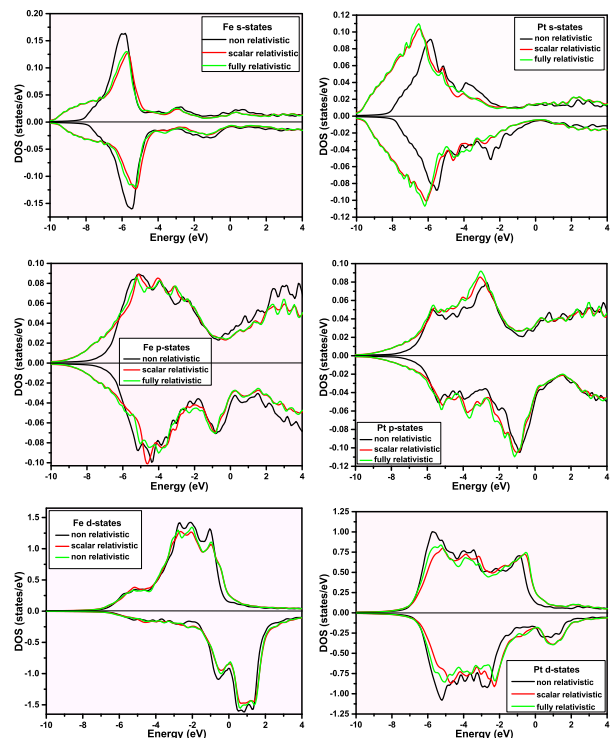


FIG. 6. Partial spin-resolved density of states for Fe and Pt sites calculated within a non-relativistic, a scalar-relativistic and a fully-relativistic framework.

from scalar-relativistic to the fully relativistic case. The largest difference between non-relativistic and relativistic case is for the s states. This may be due to the fact that s electrons have a large probability density near the nucleus where relativistic effects (mass-velocity and Darwin term) are stronger than at larger distances. Largest difference between scalar relativistic and fully relativistic calculations are for the Pt d states, where also the SOC is expected to be stronger than for the other cases.

For Pt s and d states one can make an interesting comparison with atomic results for Au (Ref. 45) which are often quoted when relativistic effects in solids are discussed. It follows from Fig. 6 that relativistic effects shift valence Pt $6s$ states to lower energies due to the orthogonality constraints to the more localized $1s$ state and Pt $5d$ states to higher energies due to a better screening of the nucleus by innermost electrons. The same happens for $6s$ and $5d$ atomic states of Au, respectively. So we can

infer that the mechanism through which relativity affects Pt states is essentially atomic-like and common to all $5d$ noble metals.

IV. DISCUSSION

Our calculations show that both computational methods give very similar values, therefore the results can be seen to represent the true LDA value of the MCA energy rather well. Our value is 3.4 meV (for the Vosko, Wilk and Nusair exchange-correlation functional).³¹ We suggest that this value is used as a benchmark for LDA calculations.

When comparing with experimental MCA energy (1.3–1.4 meV),²¹ it is clear that the LDA result does not quite agree with experiment. Clearly one has to go beyond LDA to describe the MCA energy of FePt properly. It does not matter in this respect which specific form of the LDA functional is used. Employing the generalized gradient approximation (GGA) does not help either: we obtained the MCA energy of 4.6 meV for the frequently used PBE-GGA form⁴⁶ (using the WIEN2k code and evaluating the MCA energy as a difference of total energies). It is worth to note in this respect that Shick and Mryasov were able to obtain the MCA energy of FePt as 1.3 meV by using the LDA+ U approach and searching for suitable site-related values of the U parameter.¹⁷ Interestingly, if many-body effects are described via the orbital polarization term of Brooks,⁴⁷ calculated E_{MCA} is not significantly improved in comparison with the LDA^{8,14,15,17} — despite the fact that this approach proved to be useful when calculating orbital magnetic moments of transition metals.^{48,49}

Dealing with relativistic effects via an approximate Hamiltonian with an explicit SOC term Eq. (1) as it is implemented in the WIEN2k code appears to be appropriate, provided that a sufficiently large basis for the second variation step is taken. Both treatments of relativistic effects are thus equivalent in this case.

Using different LDA functionals leads to similar but still visibly different values of E_{MCA} . Therefore, whenever theoretical values of the MCA energy are presented, it should always be stated clearly which parametrization of the LDA functional was employed.

The Bruno formula linking the MCA energy to the anisotropy of orbital magnetic moments was derived for single-component systems originally.³⁹ However, recently it was employed also for systems where there is more than one magnetic element.^{8,50–52} In our case the Bruno formula suggests a wrong magnetic easy axis, hence it not a suitable tool for understanding the MCA of FePt. As similar observations were made earlier for other compounds containing $3d$ and $5d$ elements,^{53,54} we suggest that intuition based on analysis of orbital moments should not be used for these systems.

Concerning a more detailed view on the mechanism of MCA, we found that even though MCA of FePt is dominated by a second order perturbation theory mechanism (as found earlier by Kosugi *et al.*²⁰ by analyzing the dependence of E_{MCA} of FePt on c/a), effects beyond it are clearly present as well. These effects could be identified (i) by analyzing the full angular dependence of the total energy and (ii) by inspecting how the MCA energy depends on the SOC strength. Separate scaling of SOC at Fe and Pt sites allows us to deduce that the deviations from a pure second order perturbation theory mechanism have their origin at the Pt sites.

V. CONCLUSIONS

If electronic structure calculations performed by means of FLAPW and KKR methods are properly converged, they yield the same results even for such sensitive quantities as the magnetocrystalline anisotropy (MCA) energy. The proper LDA value of the MCA energy for FePt (3.4 meV for the VWN exchange-correlation functional) is significantly larger than in experiment (1.3 meV), meaning that the MCA of FePt can be described prop-

erly only if many-body effects beyond the LDA are included. As our value of E_{MCA} was obtained by two different methods and the convergence of both of them was carefully checked, it can be used as a benchmark in future calculations.

It is not really important whether relativistic effects for FePt are accounted for by solving the full Dirac equation or whether the spin orbit coupling is treated as a correction to the scalar-relativistic Hamiltonian. The main mechanism of MCA in FePt can be described within the framework of second order perturbation theory but a significant contribution not accountable for by the second order perturbation theory is present as well.

ACKNOWLEDGMENTS

We would like to acknowledge CENTEM project (CZ.1.05/2.1.00/03.0088) and CENTEM PLUS (LO1402). Computational time has been provided with the MetaCentrum (LM205) and CERIT-SC (CZ.1.05/3.2.00/08.0144) infrastructures. In addition we would like to thank for travel support from EU-COST action MP1306 (EuSpec).

Appendix: Convergence tests

As we discussed in Sec. III B, the total energies and the MCA energy can differ by about eight or nine orders of magnitude. Therefore very well converged calculations are required for precise values of the MCA energy. In the following we check the influence of different technical parameters on the MCA energy if the WIEN2k or SPRKKR codes are used.

The E_{MCA} values presented in this Appendix sometimes differ from the values presented in the Results section (Tab. III). This is because in order to save computer resources we relied on the magnetic force theorem for evaluating E_{MCA} in this part (except for Appendix 1) while the results presented in Sec. III were evaluated by

TABLE V. Convergence of E_{MCA} obtained via the SPRKKR code with the angular momentum cutoff $\ell_{\text{max}}^{(\text{KKR})}$. E_{MCA} was evaluated by subtracting total energies.

$\ell_{\text{max}}^{(\text{KKR})}$	E_{MCA} (meV)
2.0	1.289
3.0	3.101
4.0	3.437
5.0	3.423

subtracting the total energies, as in Eq. (3). Likewise, when studying the dependence of E_{MCA} on a particular convergence parameter, the other parameters were sometimes set to lower values than what would lead to the most accurate results. These circumstances do not influence the outcome of the convergence tests.

Unless explicitly stated otherwise, the setting of technical parameters in this Appendix is the following (cf. Sec. II): $\ell_{\text{max}}^{(\text{KKR})}=3$ (for SPRKKR), $R_{\text{MT}}^{(\text{Fe})}=2.2$ a.u., $R_{\text{MT}}^{(\text{Pt})}=2.3$ a.u., $R_{\text{MT}}K_{\text{max}}=8$, $\ell_{\text{max}}^{(\text{APW})}=10$, $E_{\text{max}}=100$ Ry (for WIEN2k). Reciprocal space integrals were evaluated using a mesh of 100000 \mathbf{k} -points in the full BZ (both codes). Based on the results presented below, we argue that the numerical accuracy of our E_{MCA} calculation is about 0.1 meV.

1. Convergence of SPRKKR calculations with $\ell_{\text{max}}^{(\text{KKR})}$

It was found earlier that KKR calculations of total energies are quite sensitive to the $\ell_{\text{max}}^{(\text{KKR})}$ cutoff.^{55,56} Therefore, we explore the dependence of our results on this parameter. The results are shown in Tab. V. It follows from the table that cutting the angular momentum expansion at $\ell_{\text{max}}^{(\text{KKR})}=3$ (as it is commonly done for transition metals) yields qualitatively correct value for the MCA energy. For more accurate results, one should take at least $\ell_{\text{max}}^{(\text{KKR})}=4$.

TABLE VI. Convergence of E_{MCA} obtained via the WIEN2k code with $R_{MT}K_{max}$. E_{MCA} was evaluated by means of the magnetic force theorem.

$R_{MT}K_{max}$	E_{MCA} (meV)
6.0	2.790
7.0	3.074
8.0	2.968
9.0	2.966
10.0	3.009
11.0	2.973

2. Convergence of WIEN2k calculations with

$R_{MT}K_{max}$

An important parameter for the FLAPW calculations is the size of the basis set. It can be controlled by the $R_{MT}K_{max}$ product. The value $R_{MT}K_{max} = 7.0$ is set by default in WIEN2k. We increased the product $R_{MT}K_{max}$ step by step from 6.0 up to 11.0 and calculated the MCA energy. The results are shown in Tab. VI. It is clear from this that reliable values for the MCA energy can be obtained for a basis set determined by the $R_{MT}K_{max}=8.0$ condition.

3. Stability of WIEN2k calculations with respect to R_{MT} variations

Recently the stability of the results with respect to varying the muffin-tin radii was adopted as an informative test whether the FLAPW basis set is sufficient or not. Namely, in this way one changes the regions where the wave functions are expanded in terms of plane waves and where they are expanded in terms of atomic-like functions. Only if both expansions are appropriate the result will be stable against this variation. We adopted this test in our study, the results are summarized in Tab. VII. We can see from a good agreement between the MCA energies obtained for different muffin-tin radii settings that the basis we used for our WIEN2k calculations is appro-

TABLE VII. Dependence of E_{MCA} obtained via the WIEN2k code on muffin-tin radii R_{MT} . E_{MCA} was evaluated by means of the magnetic force theorem.

$R_{MT}^{(Fe)}$ (a.u.)	$R_{MT}^{(Pt)}$ (a.u.)	E_{MCA} (meV)
2.1	2.2	2.970
2.2	2.3	2.968
2.3	2.4	2.892

TABLE VIII. Convergence of E_{MCA} calculated by the SPRKKR and WIEN2k codes with the number of \mathbf{k} -points in the full BZ. E_{MCA} (in meV) was evaluated by means of the magnetic force theorem.

no. of \mathbf{k} -points	E_{MCA} (SPRKKR)	E_{MCA} (WIEN2k)
1000	2.893	2.930
10000	3.118	2.961
60000	3.103	2.892
100000	3.101	2.968
140000	3.100	2.896
180000	3.101	3.030
500000	3.099	2.894
800000	3.096	2.893

priate for our purpose.

4. Convergence of SPRKKR and WIEN2k calculations with the number of \mathbf{k} -points

A very important parameter is the number of \mathbf{k} -points used in evaluating the integrals in the reciprocal space. We performed corresponding tests for both codes. The dependence of E_{MCA} on the number of \mathbf{k} -points in the full BZ is shown in Tab. VIII. One can see that using about 100000 \mathbf{k} -points in the full Brillouin zone is sufficient to get reliable results.

5. Convergence of WIEN2k calculations with E_{max}

When including the SOC within the second variation step, the size of the new basis set is determined by the

TABLE IX. Convergence of E_{MCA} obtained via the WIEN2k code with E_{max} . E_{MCA} was evaluated either by subtracting total energies (the second column) or by means of the magnetic force theorem (the third column).

E_{max} (Ry)	E_{MCA} (meV)	E_{MCA} (meV)
	via E_{tot}	via force th.
2	2.640	2.941
5	4.173	3.053
10	2.334	2.960
100 (all states)	3.393	2.968

E_{max} parameter (Sec. II A). If E_{max} is sufficiently large, all scalar-relativistic eigenstates are involved. The effect of varying E_{max} on the MCA energy is shown in Tab. IX. One can see that if E_{MCA} is evaluated by means of the magnetic force theorem, it converges quite quickly with E_{max} . However, if E_{MCA} is evaluated via subtracting the total energies (i.e., via a method which is more accurate but also numerically more demanding), the convergence with E_{max} is not very good; in that case all scalar-relativistic FLAPW eigenfunctions should be included in the step where the SOC is accounted for.

¹ K. Lejaeghere, V. V. Speybroeck, G. V. Oost, and S. Cottenier, *Rev. Solid State Mater. Sci.* **39**, 1 (2014).

² “Comparing solid state dft codes, basis sets and potentials,” <http://molmod.ugent.be/deltacodesdft> (2015).

³ K. Lejaeghere, G. Bihlmayer, T. Björkman, P. Blaha, S. Blügel, V. Blum, D. Caliste, I. Castelli, S. Clark, A. D. Corso, S. de Gironcoli, T. Deutsch, J. Dewhurst, I. D. Marco, C. Draxl, M. Duak, O. Eriksson, J. Flores-Livas, K. Garrity, L. Genovese, P. Giannozzi, M. Giantomassi, S. Goedecker, X. Gonze, O. Grånäs, E. Gross, A. Gulans, F. Gygi, D. Hamann, P. Hasnip, N. Holzwarth, D. Iuan, D. Jochym, F. Jollet, D. Jones, G. Kresse, K. Koepernik, E. Küçükbenli, Y. Kvashnin, I. Locht, S. Lubeck, M. Marsman, N. Marzari, U. Nitzsche, L. Nordström, T. Ozaki, L. Paulatto, C. Pickard, W. Poelmans, M. Probert, K. Refson, M. Richter, G.-M. Rignanese, S. Saha, M. Scheffler, M. Schlipf, K. Schwarz, S. Sharma, F. Tavazza, P. Thunström, A. Tkatchenko, M. Torrent, D. Vanderbilt, M. van Setten, V. V. Speybroeck, J. Wills, J. Yates, G.-X. Zhang, and S. Cottenier, *Science*, In press (2016).

⁴ M. Asato, A. Settels, T. Hoshino, T. Asada, S. Blügel, R. Zeller, and P. H. Dederichs, *Phys. Rev. B* **60**, 5202 (1999).

⁵ J. Hu, J. Chen, and G. Ju, “L1₀ fept for magnetic recording media application,” in *Developments in Data Storage* (John Wiley and Sons, Inc., 2011) pp. 223–255.

⁶ K. R. Coffey, M. A. Parker, and J. K. Howard, *IEEE Trans. Magn.* **31**, 2737 (1995).

⁷ J. G. Gay and R. Richter, *Phys. Rev. Lett.* **56**, 2728 (1986).

⁸ P. Ravindran, A. Kjekshus, H. Fjellvåg, P. James, L. Nordström, B. Johansson, and O. Eriksson, *Phys. Rev. B* **63**, 144409 (2001).

⁹ H. J. F. Jansen, G. S. Schneider, and H. Y. Wang, in *Electronic Structure and Magnetism of Complex Materials*, edited by D. J. Singh and D. A. Papaconstantopoulos (Springer, Berlin, 2003) p. 57.

¹⁰ O. Šipr, S. Bornemann, J. Minár, and H. Ebert, *Phys. Rev. B* **82**, 174414 (2010).

¹¹ O. Šipr, S. Bornemann, H. Ebert, and J. Minár, *J. Phys.: Condens. Matter* **26**, 196002 (2014).

¹² G. H. O. Daalderop, P. J. Kelly, and M. F. H. Schuurmans, *Phys. Rev. B* **44**, 12054 (1991).

¹³ A. Sakuma, *J. Phys. Soc.* **63**, 3053 (1994).

¹⁴ I. V. Solovyev, P. H. Dederichs, and I. Mertig, *Phys. Rev. B* **52**, 13419 (1995).

¹⁵ P. Oppeneer, *J. Magn. Magn. Mater* **188**, 275 (1998).

¹⁶ I. Galanakis, M. Alouani, and H. Dreysse, *Phys. Rev. B* **62**, 6475 (2000).

¹⁷ A. B. Shick and O. N. Mryasov, *Phys. Rev. B* **67**, 172407 (2003).

¹⁸ S. Ostanin, S. A. Razee, J. B. Staunton, B. Ginatempo, and E. Bruno, *J. Appl. Phys* **93**, 453 (2003).

- ¹⁹ T. Burkert, O. Eriksson, S. I. Simak, A. V. Ruban, B. Sanyal, L. Nordström, and J. M. Wills, *Phys. Rev. B* **71**, 134411 (2005).
- ²⁰ T. Kosugi, T. Miyake, and S. Ishibashi, *Journal of the Physical Society of Japan* **83**, 044707 (2014).
- ²¹ O. A. Ivanov, L. V. Solina, V. A. Demshira, and L. M. Magat, *Phys. Met. Metallogr.* **35**, 92 (1973).
- ²² U. von Barth and L. Hedin, *J. Phys. C: Solid State Phys* **5**, 1629 (1972).
- ²³ P. Blaha, K. Schwarz, G. K. H. Madsen, D. Kvasnicka, and J. Luitz, *Wien2k, An Augmented Plane Wave plus Local orbital Program for Calculating the Crystal Properties*, <http://www.wien2k.at> (2001).
- ²⁴ H. Ebert, D. Ködderitzsch, and Minár, *Rep. Prog. Phys.* **74**, 096501 (2011).
- ²⁵ H. Ebert, *The Munich SPR-KKR package, version 7*, <http://olymp.cup.uni-muenchen.de> (2012).
- ²⁶ O. N. Mryasov, U. Nowak, K. Y. Guslienko, and R. W. Chantrell, *Europhys. Lett.* **69**, 805 (2005).
- ²⁷ J. B. Staunton, S. Ostanin, S. S. A. Razee, B. Gyorffy, L. Szunyogh, B. Ginatempo, and E. Bruno, *J. Phys. C: Solid State Phys.* **16**, S5623 (2004).
- ²⁸ O. Hovorka, S. Devos, Q. Coopman, W. J. Fan, C. J. Aas, R. F. L. Evans, X. Chen, G. Ju, and R. W. Chantrell, *Appl. Phys. Lett.* **101**, 052406 (2012).
- ²⁹ P. V. Lukashev, N. Horrell, and R. F. Sabirianov, *J. Appl. Phys.* **111**, 07A318 (2012).
- ³⁰ R. Cuadrado, T. J. Klemmer, and R. W. Chantrell, *Appl. Phys. Lett.* **105**, 152406 (2014).
- ³¹ S. H. Vosko, L. Wilk, and M. Nusair, *Can. J. Phys.* **58**, 1200 (1980).
- ³² H. Ebert, H. Freyer, A. Vernes, and G.-Y. Guo, *Phys. Rev. B* **53**, 7721 (1996).
- ³³ A. H. MacDonald and S. H. Vosko, *J. Phys. C: Solid State Phys.* **12**, 2977 (1979).
- ³⁴ J. Kuneš, P. Novák, R. Schmid, P. Blaha, and K. Schwarz, *Phys. Rev. B* **64**, 153102 (2001).
- ³⁵ A. R. Mackintosh and O. K. Andersen (Cambridge University Press, Cambridge, 1980).
- ³⁶ X. Wang, R. Wu, D.-S. Wang, and A. J. Freeman, *Phys. Rev. B* **54**, 61 (1996).
- ³⁷ J. B. Staunton, L. Szunyogh, A. Buruzs, B. L. Gyorffy, S. Ostanin, and L. Udvardi, *Phys. Rev. B* **74**, 144411 (2006).
- ³⁸ O. Šipr, S. Bornemann, H. Ebert, S. Mankovsky, J. Vackář, and J. Minár, *Phys. Rev. B* **88**, 064411 (2013).
- ³⁹ P. Bruno, *Phys. Rev. B* **39**, 865 (1989).
- ⁴⁰ G. van der Laan, *J. Phys.: Condens. Matter* **10**, 3239 (1998).
- ⁴¹ J. W. Davenport, R. E. Watson, and M. Weinert, *Phys. Rev. B* **37**, 9985 (1988).
- ⁴² G. Autès, C. Barreteau, D. Spanjaard, and M.-C. Desjonquères, *J. Phys.: Condens. Matter* **18**, 6785 (2006).
- ⁴³ J. P. Perdew and Y. Wang, *Phys. Rev. B* **45**, 13244 (1992).
- ⁴⁴ V. L. Moruzzi, J. F. Janak, and A. R. Williams, *Calculated Electronic Properties of Metals* (Pergamon, New York, 1978).
- ⁴⁵ P. Pyykko and J. P. Desclaux, *Acc. Chem. Res.* **12**, 276 (1979).
- ⁴⁶ J. P. Perdew, K. Burke, and M. Ernzerhof, *Phys. Rev. Lett* **77**, 3865 (1996).
- ⁴⁷ M. Brooks, *Physica B+C* **130**, 6 (1985).
- ⁴⁸ O. Eriksson, B. Johansson, R. C. Albers, A. M. Boring, and M. S. S. Brooks, *Phys. Rev. B* **42**, 2707 (1990).
- ⁴⁹ O. Hjortstam, J. Trygg, J. M. Wills, B. Johansson, and O. Eriksson, *Phys. Rev. B* **53**, 9204 (1996).
- ⁵⁰ F. Gimbert and L. Calmels, *Phys. Rev. B* **86**, 184407 (2012).
- ⁵¹ S. Assa Aravindh, S. Mathi Jaya, M. C. Valsakumar, and C. S. Sundar, *Appl. Nanosci.* **2**, 409 (2012).
- ⁵² M. Kotsugi, M. Mizuguchi, S. Sekiya, M. Mizumaki, T. Kojima, T. Nakamura, H. Osawa, K. Kodama, T. Ohtsuki, T. Ohkochi, K. Takanashi, and Y. Watanabe, *J. Magn. Magn. Materials* **326**, 235 (2013).
- ⁵³ C. Andersson, B. Sanyal, O. Eriksson, L. Nordström, O. Karis, D. Arvanitis, T. Konishi, E. Holub, Krappe, and J. H. Dunn, *Phys. Rev. Lett.* **99**, 177207 (2007).
- ⁵⁴ O. Šipr, J. Minár, S. Mankovsky, and H. Ebert, *Phys. Rev. B* **78**, 144403 (2008).
- ⁵⁵ R. Zeller, *J. Phys.: Condens. Matter* **25**, 105505 (2013).
- ⁵⁶ A. Alam, S. N. Khan, A. V. Smirnov, D. M. Nicholson, and D. D. Johnson, *Phys. Rev. B* **90**, 205102 (2014).